# THE FLOW OVER ASYMMETRICAL RIPPLES:
# AN EXPERIMENTAL INVESTIGATION ON THE HYDRODYNAMICS BEHAVIOR

Carmelo Petrotta[1], Carla Faraci[2], Pietro Scandura[3], Enrico Foti[4]

## Abstract

This paper reports on an experimental campaign focused on the hydromorphodynamics induced by sea waves propagating over a sloping sandy bed. The slope triggers a flow asymmetry that reflects on the bedform characteristics. Hydrodynamic characteristics have been acquired by means of a Vectrino Profiler at two measurement sections, one located over the sloping bed, the other at the plane bottom. The velocity measurements showed that waves are strongly skewed, with flat, wide troughs and sharp crests. As a consequence, phase averaged velocity profiles exhibit onshore velocities greater than offshore ones. An offshore-directed steady current occurs, which near the bed is strongly influenced by the ripple-generated lee wake vortices.

**Key words:** hydrodynamics, sediment transport, morphodynamics, ripples, bottom boundary layer, steady current

## 1. Introduction

Seabeds are often covered by small sedimentary structures known as ripples. Such bedforms induce a substantial modification of the bottom roughness with repercussions on the hydrodynamics especially inside the boundary layer.

Due to their impacts on the near shore flow field, many researchers focused their studies on the prediction of ripple characteristics in order to have insights on sediment transport and wave attenuation over a sand bottom. Among them, Nielsen (1981), Wiberg and Harris (1994), Faraci and Foti (2002), Grasmeijer and Kleinhans (2004) performed a large number of laboratory investigations on ripple geometry in order to propose ripple predictor models based on the flow parameters.

At full scale conditions, O'Donoghue et al. (2006) showed significant differences in the ripple size compared with earlier results obtained in small scale installations. They also found that, depending on the sand median grain size, a lack of equilibrium conditions could occur. Moreover Doucette and O'Donoghue (2006) investigated the effects of varying the flow conditions on ripple characteristics.

On the theoretical side, Blondeaux et al. (2000) investigated ripple formation by means of a linear stability analysis and found that because of the presence of a steady velocity component in the direction of wave propagation, ripples migrate at a constant rate depending on sediments and wave characteristics. In particular this current arises both because of the spatial non uniformity of the boundary layer and by the wave skewness induced by wave nonlinearities.

All the mentioned studies dealt with bedforms generated over horizontal sandy bottoms. However, sand ripples have been frequently observed over sloping beds where the wave characteristics may be different from those of a wave over an horizontal bed. Indeed, due to the interaction with the sloping bed, waves become asymmetric, with a steep front and a gently sloping rear face. Such a phenomenon has repercussions also on the near bed acceleration, which is larger in the onshore direction, giving rise to an acceleration-skewed flow. Wave skewness and asymmetry have a strong impact on both hydrodynamics and sediment transport near the coast (Cavallaro et al., 2011; Scandura et al, 2016).

In these conditions also sea bed ripples become asymmetric in shallow water regions. The asymmetry of flows and ripples is considered to exert crucial influences on the direction and the net rate of sand transport

---
[1] Department of Engineering, University of Messina, Italy. cpetrotta@unime.it
[2] Department of Engineering, University of Messina, Italy. cfaraci@unime.it
[3] Department of Civil Engineering and Architecture, University of Catania, Italy. pscandu@dica.unict.it
[4] Department of Civil Engineering and Architecture, University of Catania, Italy. efoti@dica.unict.it

(Sato and Horikawa, 1986). In particular, the latter authors showed that the ripples are asymmetric under skewed oscillatory flows with the onshore flank of the ripples steeper than the offshore one. This observation has been recently confirmed by Blondeaux et al (2015), who performed a weakly nonlinear stability analysis of a flat sandy bottom subjected to an oscillatory flow, in order to relate the symmetry index of the ripples to wave and sediment characteristics. Indeed they found that the characteristic profile of sea ripples affected by a steady current can be recognized from the lee side of the ripples being steeper than the stoss side.

Measurements in an oscillatory water tunnel over sand ripples were carried out by van der Werf et al. (2007). They reported that the asymmetry of the oscillatory flow produces steady circulation cells with a dominant offshore mean flow. They also showed that velocity skewness induces a net suspended load flux in the offshore direction while the net bed load sediment flux was onshore with a corresponding onshore ripple migration.

In this paper the results of an experimental campaign aimed at recovering both the morphodynamics and the hydrodynamics generated by waves propagating over an uneven sloping bed in a wave flume are presented. Whereas morphodynamic characteristics have been discussed in detail in Faraci et al. (2016), in this paper the attention is focused on the hydrodynamic behaviour of the flow on the sloping bed in the presence of ripples. The paper is organized as follows. First the experimental set up and procedure is presented. Then the experiments are described and the experimental results are examined. The paper ends with some conclusions.

## 2. Experimental set up and procedure

The experimental campaign which focused on the interaction between asymmetrical oscillatory flows and rippled beds, was performed in the hydraulic laboratory of the University of Messina (Italy). Experiments were carried out in a wave flume 18.5 m long, 0.4 m wide and 0.8 m high with flat stainless steel bottom and glass walls (Figure 1a).

Waves are generated within the flume by means of a flap type wavemaker which is able to reproduce both regular and random waves characterized by wave heights up to 0.12 m and wave periods between 0.5 and 2 s. The wavemaker was driven by a pneumatic system and was electronically controlled. In the present campaign regular waves were generated, setting the signal frequency, amplitude and offset position by a dedicated software.

At the back of the wavemaker some mattresses of creased pipe pieces were placed to absorb any spurious reflection caused by the flap. More details on the experimental setup can be found in Liu and Faraci (2014) and Faraci et al. (2015).

Starting at 8 m away from the wavemaker and for the remaining flume length, the bottom was covered with a layer of 0.2 m thick of uniform sand, characterized by a median grain size $d_{50}$=0.25 mm. A plane beach, 3.5 m long with a slope of 1:10, was built oppositely to the wavemaker in order to minimize reflection. Moreover the plane beach had the role of triggering the asymmetry of the waves propagating along the flume.

In the present campaign regular waves characterized by heights between 1 and 10 cm and periods between 0.8 and 1.4 s were generated and propagated along the flume and their effect on the sandy bed was analyzed.

Measurements of wave characteristics throughout the wave flume were performed by means of five resistive wave gauges. The first one was located 3.25 m off the wavemaker, three of them were placed on the horizontal sand layer and spaced in such a way to allow the wave reflection along the flume to be evaluated by means of Mansard and Funke's (1980) method. The last one was located on the sloping beach where the waves shoal.

Velocity profiles were acquired by means of a Vectrino Profiler (Nortek As.) in two sections, the first one located 1.5 m far from the beginning of the sandy bed (Section $S_1$) and the second one located 1.1 m after the beginning of the slope (Section $S_2$). The sampling volume of the probe extends from 40 mm up to 74 mm below the transducer, including 34 measuring points with 1 mm resolution and sampling rate equal to 100 Hz. In order to obtain reliable flow measurements, the Signal to Noise Ratio (SNR) has been kept greater than 30 dB at every measuring point; it is possible to increase SNR by increasing the cell size

parameter. In one of the performed tests ($DT_7$) the velocity profiles were acquired once with a cell size parameter equal to 1 mm and a second time increasing the cell size from 1 to 2 mm. However, relevant differences were not observed comparing the two obtained profiles.

Moreover, the cell where SNR reaches the greatest value is located 5.5 cm below the transducer tip, i.e. in the middle of the measured sampling volume. Hence, each measurement station along the profile was overlapped with the lower one by a 15 mm layer, in order to better control the lower part of the sampled volume which is affected by high reflections from the bottom and low SNR. Finally, velocity profiles were smoothed out by a simple moving average with 15 data window length.
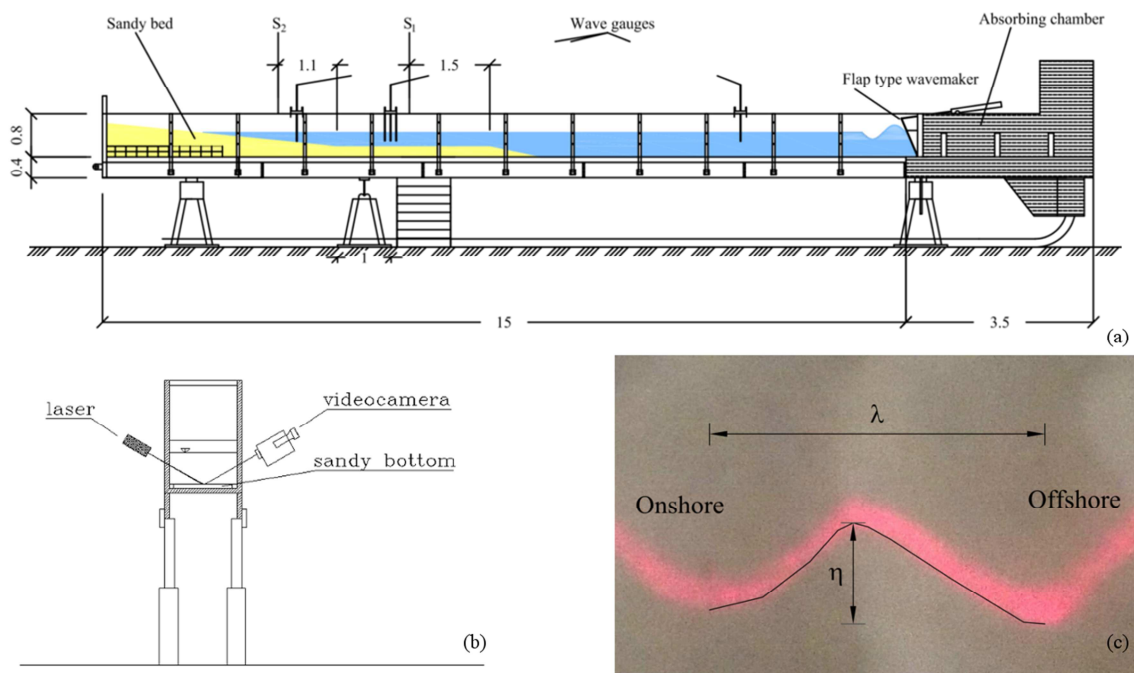


Figure 1. Experimental set up adopted in the present experimental campaign (a); sketch of the optical structured light technique (b); example of the laser light on the sandy bottom with the two half-wavelength λ+ and λ- (c).

The bed morphology was acquired by means of a structured light optical system (see Faraci and Foti, 2002 or Faraci et al., 2012 for details on the technique). The light sheet optically slices the measured body creating a cross-sectional image that can be observed and recorded through a video camera and then analyzed to obtain the ripple dimensions (Figure 1 (b) and 1 (c)).

Once the image was gathered by the video camera, suitable image processing procedures was adopted, in particular the correspondence between the image units, given in pixels, and the object dimensions were preliminary stated. This task was accomplished by acquiring the image of a known object and deriving the coefficients which give the unit dimension of one pixel in both horizontal and vertical directions.

Each experiment required some preliminary operations, i.e. the definition of the control parameters to be provided to the wavemaker in order to generate the desired wave, the choice of the Vectrino profiler software configuration, the calibration of the optical system, the leveling of the sandy bed. This last task had to be carefully performed in order to remove any ripple mark from the sandy bed and to start each experiment from an initially flat condition.

Hydrodynamic and morphodynamic measurements had to be acquired separately. Indeed the flow measurements required enough suspension in order to allow the acoustic signal to be reflected by the suspended particles. The morphodynamic measurements instead had to be performed in perfectly clear water to make the image formation possible on the camcorder lenses. Thus the experimental procedure followed such a schedule:

- In the presence of clear water and starting from an initially flat bed, the waves propagated on the sandy bottom and triggered the formation of ripple bedforms. In the same time the structured light approach was used to acquire the rippled bed images by means of a camera. The morphodynamic

acquisition ended once the equilibrium was achieved, which generally occurred within 15 minutes.
- Once the morphodynamic measurements were performed, the water was seeded by means of talc powder and two vertical profiles were acquired, the first one located on the horizontal sandy bottom ($S_1$), the other one on the sloping bed ($S_2$).

A post-processing stage was then performed in order to interpret the acquired images according to the optical technique with the aim of determining their dimensions.

## 3. Analysis of the results

### 3.1 *Experiments*

Ten experiments were performed in the presence of regular waves. In Table 1 the experimental parameters of each test are reported. In particular the first column indicates the test name, then the second column reports the water depth and the last two columns the wave height and the period. It is worth pointing out that the water depth is measured on the sloping bottom at the cross section where ripple characteristics are measured. On the horizontal bed (section $S_1$) the water is 10 cm deeper than on the sloping measurement section ($S_2$).

Table 1. Hydraulic characteristics of the performed experiments.

| Test name | d [m] | H [m] | T [s] |
|---|---|---|---|
| $CF_1$ | 0.1450 | 0.0675 | 1.2324 |
| $DT_7$ | 0.1450 | 0.0694 | 1.2183 |
| $DT_5$ | 0.1450 | 0.0713 | 1.0100 |
| $DT_4$ | 0.1450 | 0.0825 | 1.0100 |
| $AB_4$ | 0.1450 | 0.1006 | 1.0101 |
| $DT_1$ | 0.1450 | 0.0573 | 0.8412 |
| $LM_1$ | 0.1450 | 0.0958 | 0.8402 |
| $LM_2$ | 0.1450 | 0.0911 | 0.8400 |
| $DT_3$ | 0.1470 | 0.1270 | 0.8399 |
| $AB_8$ | 0.1450 | 0.1217 | 0.8400 |

In Figure 2 an example of the water elevation, as recorded by the wave gauge located onshore, i.e. at the beginning of the sloping beach, is reported for the two regular wave tests named $DT_3$ and $DT_4$.

The dimensionless parameters usually employed in the analysis of ripple dynamics are:
- the relative density of sediments:

$$s = \frac{\rho_s}{\rho} \qquad (1)$$

- the flow Reynolds number:

$$\mathrm{Re} = \frac{U_0 A}{\nu} \qquad (2)$$

- the sediment Reynolds number:

$$\mathrm{Re}_d = \frac{U_0 d_{50}}{\nu} \qquad (3)$$

- the mobility number:

$$\psi = \frac{U_0^2}{(s-1)g d_{50}} \qquad (4)$$

- the Shields parameter (related to the mobility number):

$$\vartheta_{2.5} = \frac{1}{2} f_w \frac{U_0^2}{(s-1)gd_{50}} \tag{5}$$

Where:
- $\rho_s$ is the sediment density;
- $\rho$ is the water density;
- $U_0$ is the orbital velocity;
- A is the orbital amplitude;
- $\nu$ is the kinematic water viscosity;
- $d_{50}$ is the median grain size;
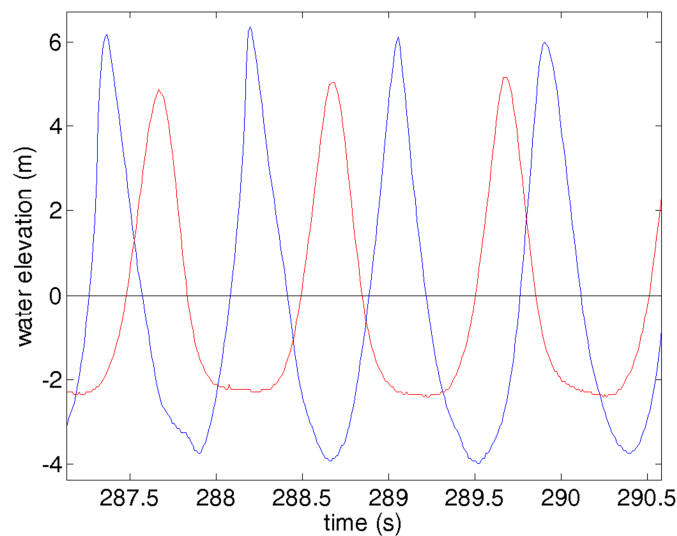- $f_w$ is the friction factor defined in terms of Re and $A/d_{50}$.



Figure 2. An example of the water elevation for two regular wave tests (blue line: test $DT_3$: H=0.12 m; T=0.84 s; red line: test $DT_4$: H=0.082 m; T=1.00 s).

### 3.2 *Experimental results*

In this section, the hydrodynamic characteristics of the flow generated by waves propagating over the sloping sandy bed are analyzed. As previously mentioned, also the morphodynamic characteristics of the ripples were measured and discussed in a companion paper (Faraci et al. 2016). Here for sake of brevity only some brief mentions are included below for the morphodynamics.

In Table 2 the ripple characteristics at the equilibrium, namely the ripple wavelength $\lambda$, the ripple height $\eta$ and their velocity of migration $v_o$ are reported for each test. Table 2 also reports the main dimensionless parameters previously mentioned. In particular, the last three columns indicate the flow Reynolds number, the sediment Reynolds number and the mobility number respectively. The sediment relative density was constant and equal to s=2.65 throughout the experimental campaign, thus it is not included in the table.

#### 3.2.1 *Morphodynamic evolution*

The seabed around sections $S_1$ and $S_2$ becomes rippled after the propagation of few tens of waves. The evolution of ripple wavelength $\lambda$ and height $\eta$ at section $S_2$ is shown in Figure 3 (a) for tests $DT_3$ and $DT_4$. During experiment $DT_4$, ripple wavelength reached immediately a value close to equilibrium one $\lambda_{eq}$. Then, it seems that ripple wavelength oscillated, damping slowly, around a slightly sloping straight line. During experiment $DT_3$, an almost linearly increase of the wavelength is observed within the first minute ($\lambda \cong 2/3 \lambda_{eq}$) and at about 11 min the equilibrium value was reached.

Table 2. Morphodynamic characteristics of the performed experiments.

| Test name | λ [m] | η [m] | $v_o$ [cm·min$^{-1}$] | Re | $Re_d$ | ψ |
|-----------|-------|-------|----------------------|-----|--------|----|
| $CF_1$ | 0.0607 | 0.0148 | 0.0375 | 5388.8560 | 45.7716 | 8.2870 |
| $DT_7$ | 0.0526 | 0.0096 | 0.1133 | 5173.2583 | 49.1782 | 9.5664 |
| $DT_5$ | 0.0528 | 0.0088 | 0.0012 | 4537.8682 | 46.0619 | 8.3924 |
| $DT_4$ | 0.0571 | 0.0086 | -0.2118 | 6357.4961 | 54.5172 | 11.7563 |
| $AB_4$ | 0.0617 | 0.0073 | -0.1321 | 31333.6701 | 99.9217 | 39.4933 |
| $DT_1$ | 0.0334 | 0.0043 | -0.1521 | 2153.8072 | 31.7091 | 3.9771 |
| $LM_1$ | 0.0393 | 0.0076 | -0.0814 | 3682.2533 | 37.8378 | 5.6631 |
| $LM_2$ | 0.0434 | 0.0074 | -0.6836 | 5504.2975 | 46.2616 | 8.4653 |
| $DT_3$ | 0.0527 | 0.0070 | -0.4050 | 6179.0165 | 53.7401 | 11.4235 |
| $AB_8$ | 0.0400 | 0.0060 | -0.0435 | 7490.7005 | 49.1376 | 9.5506 |

The velocity of migration measured at the ripple crest was plotted as a function of time in Figure 3 (b). Migration velocity was considerably negative during first 4'30'' of $DT_4$ test. After that, velocity started oscillating around zero, therefore it seems that ripples found an equilibrium position.

The direction of the migration velocity changed repeatedly during first 3 – 4 minutes of test $DT_3$. Then it started slightly growing in offshore direction until the end of the experiment. However further investigations are needed in order to explain the differences in the migration velocity and the achievement of the equilibrium position.
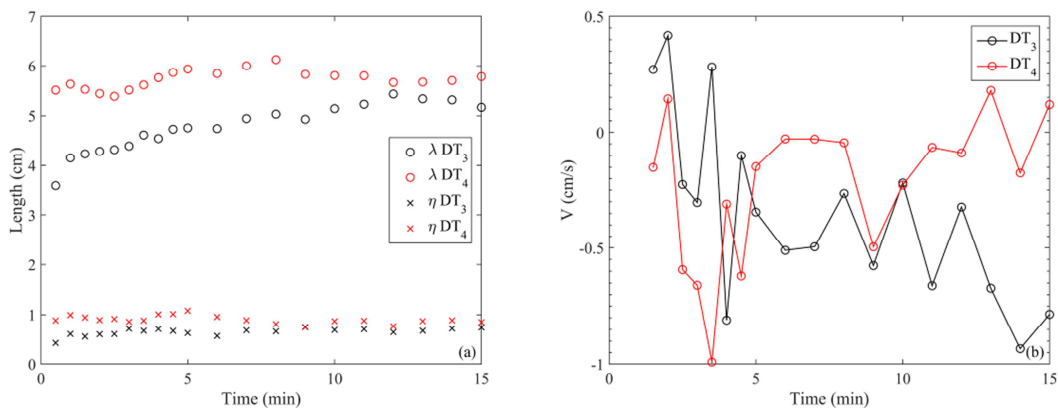


Figure 3. Evolution of the morphodynamic quantities measured during tests $DT_3$ (red markers) and $DT_4$ (black markers): (a) ripple wavelength and height; (b) migration velocity of ripple crests.

### 3.2.2 *Hydrodynamic evolution and phase averaged velocity profiles*

In Figure 4 the cross-shore velocities at an elevation of 1.5 cm above the bed (about 0.5 cm over ripple crest) measured during experiments $DT_3$ and $DT_4$ are shown respectively in panel a) and b). In Figure 4 the moving averaged velocities $V_{MA}$ determined by averaging over 1 period is also shown. It can be observed that a negative (offshore-directed) steady current appears. The steady current contributes to offshore migration as described in the previous sections. However some other mechanisms, such as the wave asymmetry should play a role in the ripple migration as well and need further investigations.
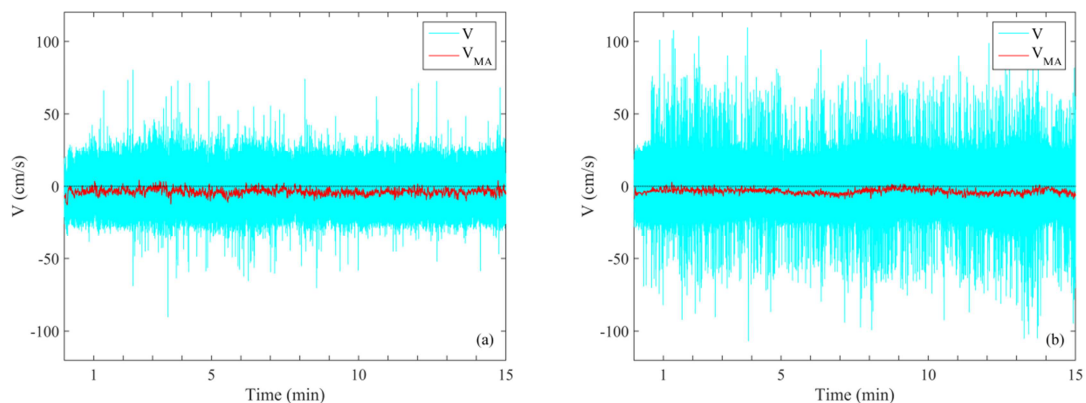
Figure 4. Cross-shore velocities measured at section $S_1$: panel (a) shows test $DT_3$ (H=0.1270 m; T=0.84); panel (b) shows test $DT_4$ (H=0.0825 m; T=1.01 s).

Although height and frequency of the $DT_3$ test are greater than $DT_4$ ones, higher mean velocities are achieved during the latter experiment. Such evidence occurs at all the different elevations, as it can be observed in Figures 6 and 7. This evidence agrees with the achievement of a more rapid morphodynamic equilibrium condition during $DT_4$ experiment rather than during $DT_3$ experiment, as it has been observed looking at Figure 3.

Velocity profiles have been acquired along the water column by moving the sensor up by a fixed amount $\Delta z$ during each experiment. As said before, in order to filter out the lower layer of the sampling volume, in most of the tests $\Delta z$ has been kept equal to 2 cm, but in some tests it was reduced to 1 or 0.5 cm in order to check the proper overlap between the profile segments in the reconstruction of the velocity profile.

The signal acquired by each cell of the Vectrino Profiler was analyzed by a zero up-crossing method, decomposed and phase-averaged in 16 phases spaced of $\pi/8$ to obtain phase averaged velocity profiles. Only 4 phases are shown here to avoid overcrowding of points.

A simple moving average including the points spatially falling within ±2mm (window length = 15) filter is applied to raw data, whose dispersion is indicated by some error bars. Data scattering is greater near the bottom where Vectrino Profiler accuracy decreases due to seabed reflection and bed motion during measurements.

Figures 5 – 7 depict the velocity profiles of the experiments $DT_5$, $DT_4$, $DT_3$, respectively at the sections $S_1$ (plane bed) and $S_2$ (sloping bed). The four phase averaged velocity profiles are: the first one at $\pi/2$ (wave crest), the second at $\pi$, then at $3\pi/2$ (wave trough) and finally at $2\pi$, that corresponds to the zero up-crossing. Moreover the mean velocity profile $v_{avg}$ is also shown. The wave asymmetry causes that zero down-crossing is reached before the $\pi$ phase.

Profiles disclose that wave is strongly asymmetrical, indeed $\pi/2$ phase profile shows larger velocities than $3\pi/2$ one, notwithstanding the consideration that mean velocity profile is almost negative throughout the water column. This is also confirmed by looking at the surface elevation of Figure 2, where waves exhibit higher peaked and narrow crests and smaller broad troughs.

Velocity profiles acquired at sections $S_2$ (shallower) are greater than ones measured at section $S_1$ (deeper). This also depends on the shoaling process that concentrates the energy flux on a smaller water depth. Velocity growth cause the thickening of the boundary layer (van der A et al., 2011).

All the presented velocity profiles exhibit offshore directed steady currents, that however behave differently close to the bed in the three investigated cases: indeed in the test $DT_5$ it is slightly positive up to about 2 cm from the bed. In test $DT_4$ a negative mean velocity profile can be observed everywhere. Such occurrence also justifies the offshore directed ripple migration, observed during this experiment. Finally test $DT_3$ (section $S_1$) exhibits a significant near bed positive (onshore-directed) steady current. At section $S_2$ however such a positive near bed mean velocity is not observed.

Near the bed the higher offshore mean velocity of $DT_4$ is due to a mechanism similar to that described in Scandura (2007), Cavallaro et al. (2011) and Scandura et al. (2016). Due to the large wave asymmetry (see Figure 2) the intensity of turbulence is different in the two half-cycles. Therefore the time average of the

Reynolds stresses does not vanish at each elevation. The mean Reynolds stresses are balanced by the mean viscous stress arising from the velocity profile of the steady current.

Fredsøe et al. (1999) observed that period averaged velocity profiles near the bed at four measurement sections along the ripple profiles exhibit different behaviours, being positive at the stoss side of ripples and negative at the lee side. Such observation has been related to the presence of recirculating cells induced by the presence of the ripple itself.



Figure 5. Phase averaged velocity profiles at sections $S_1$ (a) and $S_2$ (b) (test $DT_5$: H=0.0713 m; T=1.01 s).
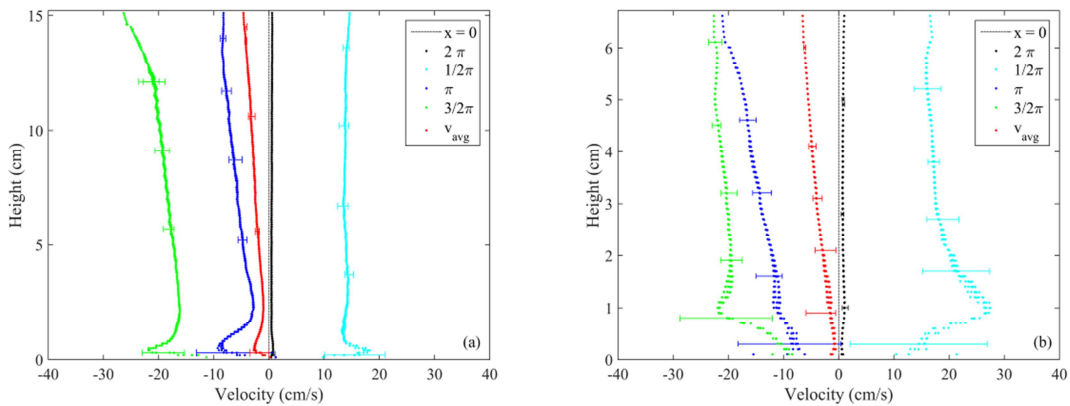


Figure 6. Phase averaged velocity profiles at sections $S_1$ (a) and $S_2$ (b) (test $DT_4$: H=0.0825 m; T=1.01 s).
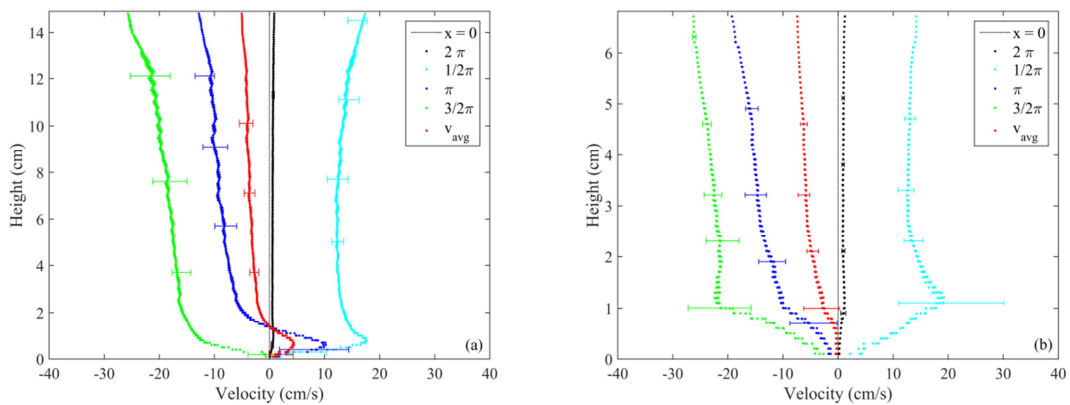


Figure 7. Phase averaged velocity profiles at sections $S_1$ (a) and $S_2$ (b) (test $DT_3$: H=0.1270 m; T=0.84 s).

In order to further investigate the differences between Figures 5-7, a more detailed velocity mapping has been performed along the ripple profile.

In particular Figure 8 shows the velocity profiles obtained at section $S_2$ at four different measurement stations along the ripple profile, whose wavelength is 2.5 cm. The four stations are at ripple crest (Figure 8a), at an intermediate position between crest and the offshore trough, horizontally spaced from the first one by 0.5 cm (Figure 8b), at ripple trough, horizontally spaced of 0.75 from the previous one (Figure 8c) and finally at the intermediate section between the trough and the offshore crest, i.e. further spaced by 0.5 cm (Figure 8d).

Looking at mean velocity profiles, a small positive steady current comes up above the crest (a), it grows on the lee ripple side (b), it disappears above the trough (c) and it becomes negative above the stoss side of the ripple (d).

The presence of such steady currents near the bed may be linked to the motion of lee-wake vortex as before discussed and seems to confirm the findings of Fredsøe et al., (1999).
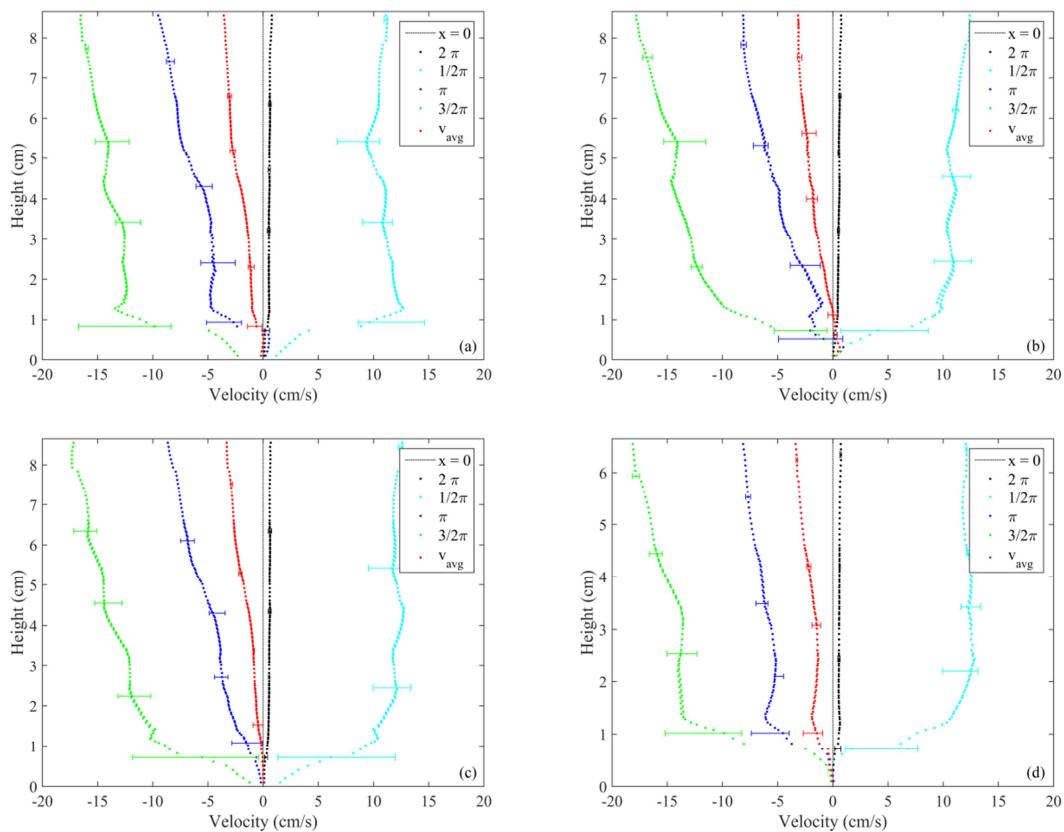


Figure 8. Phase averaged velocity profiles at four measurement stations (test $DT_1$: H=0.0573 m; T=0.84 s). (a) ripple crest; (b) intermediate station between crest and trough; (c) ripple trough; (d) intermediate station between the trough and the adjacent crest.

## 4. CONCLUSIONS

In this paper the preliminary analyses performed on the data acquired in an experimental campaign aimed at investigating the flow field generated by the propagation of regular waves over a sloping sandy bed are described. Flow field was measured by means of a Vectrino Profiler in order to analyse how the wave-sloping bed interaction affects its hydrodynamics.

Phase averaged velocity profiles acquired at the plane bed test section $S_1$, together with ones measured at

the sloping test section $S_2$, show that wave is strong skewed, with flat, wide troughs and sharp crests. Therefore, the phase averaged velocity profile exhibit an offshore-directed steady current together with onshore velocities ($\pi/2$ phase) greater than offshore ones ($3\pi/2$ phase).

This offshore current is due to the undertow but near the bed is larger when the wave skewness is larger because of the asymmetry of turbulence in the two half cycles.

It was observed that period averaged velocities measured near the bed are positive at the stoss side of the ripple and negative at the lee side, indicating the existence of two recirculating cells induced by the presence of the ripple itself.

## Acknowledgements

## References

Blondeaux P., Foti E., Vittori G., 2000. Migrating sea ripples. *Eur. J. Mech. B - Fluids* 19, 285–301.

Blondeaux, P., Foti, E., and Vittori, G., 2015. A theoretical model of asymmetric wave ripples. *Philosophical Transactions of the Royal Society of London A: Mathematical, Physical and Engineering Sciences*, 373 (2033), 20140112.

Cavallaro, L., Scandura P., Foti E., 2011. Turbulence-induced steady streaming in an oscillating boundary layer: on the reliability of turbulence closure models. *Coastal Engineering*, 58(4), 290-304.

Doucette, J. S. And O'Donoghue, T., 2006. Response of sand ripples to change in oscillatory flow. *Sedimentology*, 53: 581–596.

Faraci, C. and Foti, E., 2002. Geometry, migration and evolution of small-scale bedforms generated by regular and irregular waves. *Coast. Engng.*, 47: 35–52.

Faraci, C., Foti, E., Marini A., Scandura, P., 2012. Waves Plus Currents Crossing at a Right Angle: Sandpit Case, *J. Waterway, Port, Coast. and Ocean Eng.,* 138(5).

Faraci, C., Scandura, P., and Foti, E., 2015. Reflection of sea waves by combined caissons. *J. Waterway, Port, Coast. and Ocean Eng.,* 141(2).

Faraci, C., Petrotta C., Scandura, P., Foti, E., and Blondeaux P., 2016. The flow over asymmetrical ripples: an experimental investigation on the morphodynamic behavior , *Proc. 35ᵗʰ Conf. on Coastal Eng.* (under review)

Fredsøe, J., Andersen, K. H., and Sumer, B. M., 1999. Wave plus current over a ripple-covered bed. Coastal Engineering, 38(4): 177-221.

Grasmeijer, B.T. and Kleinhans, M.G., 2004. Observed and predicted bed forms and their effect on suspended sand concentrations. *Coast. Engng.*, 51(5): 351-371.

Liu, Y. and Faraci, C., 2014. Analysis of orthogonal wave reflection by a caisson with open front chamber filled with sloping rubble mound. *Coast. Engng.*, 91:151–163.

Mansard, E. P. D., and Funke, E. R., 1980. The measurement of incident and reflected spectra using a least squares method. *Proc., 17th Int. Coastal Engineering Conf.*, ASCE, New York: 154–172.

Nielsen, P., 1981. Dynamics and geometry of wave-generated ripples. *J. Geophys. Res.* 86 (C7): 6467– 6472.

O'Donoghue, T., Doucette, J. S., Van der Werf, J. J., and Ribberink, J. S., 2006. The dimensions of sand ripples in full-scale oscillatory flows. *Coastal Engineering*, 53(12), 997-1012.

Sato, S. and K. Horikawa, 1986. Laboratory study on sand transport due to asymmetric oscillatory flows, *Proc. 20th Conf. on Coastal Eng.*: 1481-1495.

Scandura, P., 2007. Steady streaming in a turbulent oscillating boundary layer. *J. Fluid Mech.*, 571, pp. 265–280

Scandura, P., Faraci, C., and Foti, E., 2016. A numerical investigation of acceleration-skewed oscillatory flows *J. Fluid Mech.* 808: 576-613.

Van der A, D., O'Donoghue, T., Davies, A. G., and Ribberink, J. S., 2011. Experimental study of the turbulent boundary layer in acceleration-skewed oscillatory flow. *Journal of fluid mechanics*, 684 (251).

Van der Werf, J. J., Doucette, J. S., O'Donoghue, T., and Ribberink, J. S., 2007. Detailed measurements of velocities and suspended sand concentrations over full-scale ripples in regular oscillatory flow, *J. Geophys. Res.,* 112, F02012

Wiberg, P.L. and Harris, C.K., 1994. Ripple geometry in wave-dominated environments. *J. Geophys. Res.*, 99(C1): 775–789.